arXiv:cond-mat/0507370v2 [cond-mat.stat-mech] 1 Nov 2005

Caging and mosaic lengthscales in plaquette spin models of glasses

Robert L. Jack[1] and Juan P. Garrahan[2]

[1]*Rudolf Peierls Centre for Theoretical Physics, University of Oxford, 1 Keble Road, Oxford, OX1 3NP, UK*
[2]*School of Physics and Astronomy, University of Nottingham, Nottingham, NG7 2RD, UK*

We consider two systems of Ising spins with plaquette interactions. They are simple models of glasses which have dual representations as kinetically constrained systems. These models allow an explicit analysis using the mosaic, or entropic droplet, approach of the random first-order transition theory of the glass transition. We show that the low temperature states of these systems resemble glassy mosaic states, despite the fact that excitations are localized and that there are no static singularities. By means of finite size thermodynamics we study a generalised caging effect whereby the system is frozen on short lengthscales, but free at larger lengthscales. We find that the freezing lengthscales obtained from statics coincide with those relevant to dynamic correlations, as expected in the mosaic view. The simple nucleation arguments of the mosaic approach, however, do not give the correct relation between freezing lengths and relaxation times, as they do not capture the transition states for relaxation. We discuss how these results make a connection between the mosaic and the dynamic facilitation views of glass formers.

PACS numbers: 64.60.Pf, 75.10.Hk

I. INTRODUCTION

The aim of this paper is to study possible connections between two perspectives on the glass transition [1]. One is the mosaic, or entropic droplet, view that follows from the random first-order transition theory of Kirkpatrick, Thirumalai and Wolynes (KTW) [2, 3]: a deeply supercooled liquid is viewed as a patchwork of correlated mesoscopic regions which relax by entropically driven nucleation events. These "mosaics" are characterised by a length scale that diverges on approach to a temperature T_K, where a Kauzmann [4, 5] entropy crisis occurs. The growth of static correlations, under certain assumptions for droplet nucleation, leads to a divergence of relaxation times of the Vogel-Fulcher kind [1] in three dimensions.

The second, in principle very different, approach is based on the idea of dynamic facilitation [6, 7]: glassiness is not due to any precipitous thermodynamics, but is a consequence of effective constraints in the dynamics. Here, the central feature is dynamic heterogeneity [8, 9], and the corresponding dynamic scaling, i.e., growing times are accompanied by growing dynamic, but not necessarily static, correlation lengths [10]. In this view there are no finite temperature singularities, and scaling properties are controlled by zero temperature critical points where dynamic lengths and times diverge [11]. The simplest models that realize this perspective are kinetically constrained lattice models, such as the facilitated spin models of Fredrickson and Andersen (FA) and Jackle's East model [6, 12, 13].

Here we study lattice spin models with plaquette interactions [14, 15, 16, 17] from the mosaic or entropic droplet perspective. The two models we consider are the square plaquette model (SPM) [14, 15] and the triangular plaquette model (TPM) [16, 17]. These models have exact dual descriptions: one in terms of interacting spin variables with standard single-spin Glauber dynamics; another in terms of free excitations with dynamics subject to kinetic constraints. The dynamics of the SPM is like that of the facilitated FA model [15], the dynamics of the TPM, like that of the East model [17].

While plaquette models are realizations of the dynamic facilitation scenario, they also allow for a detailed and explicit analysis using the mosaic approach. They therefore allow a direct analysis of the similarities and differences between the facilitation and the mosaic perspectives on glasses. In this work, we apply to these models the procedure recently suggested by Bouchaud and Biroli (BB) [18], by which the mosaic lengthscale is estimated from the partition function of finite droplets within a larger system. We show that low temperature states do resemble mosaic states, and that the associated lengths can be extracted using the BB procedure. We also show that these thermodynamic lengthscales have the same scaling as those extracted from bulk many-point static correlations, and from multi-point dynamical correlation functions which measure dynamic heterogeneity. In the case of the SPM, the static analysis gives two typical caging lengths, a feature not anticipated in BB. Moreover, the relation between caging lengths and relaxation times in these models is not that expected from the mosaic approach, as the nucleation assumptions miss the relevant transition states and overestimate the free-energy barriers to droplet melting.

The paper is organized as follows. In section II we give a summary of the arguments of KTW and BB, and make general observations about the applicability of this approach to the models studied in this work. In section III we apply the mosaic procedure to the SPM, and compare the lengthscales obtained with other relevant static and dynamic lengths of the system. In section IV we repeat the analysis for the TPM. Finally, in section V we give our conclusions.

II. BACKGROUND

A. Mosaics and their lengthscales

The basic arguments underlying the BB procedure to compute a mosaic lengthscale are the following [2, 18].

Imagine a glassy state in which an atom is prevented from moving by the fact that its neighbours are fixed in position. This picture is consistent only insofar as the neighbours of the original atom are fixed by their neighbours, and so on. Consider now the original atom and its neighbours as a small droplet. One can compute the probability that the droplet can relax, assuming that its boundaries are fixed. If this probability is small then rearrangements require correlated motion over distances larger than this droplet. One must then increase the droplet size and recalculate the probability of rearrangement. In a system with finite-ranged interactions, as the droplet is made larger, we eventually cross over to a regime where the rearrangement probability is large. All larger droplets will be then able to rearrange by sequential moves of this type.

This crossover defines the mosaic lengthscale [2, 18]. The result is a picture of a glassy state in which droplets of small sizes are jammed, or frozen, by their boundaries, whereas those with large sizes are unjammed, or melted. As the temperature decreases, the typical lengthscale separating jammed and unjammed droplets increases. (The idea of using finite size scaling to extract a lengthscale is not at all new, of course. See Refs. [19, 20] for applications to glass formers.)

The above remarks can be made quantitative by way of three assumptions [2, 18]:

(i) A droplet of size ξ contains very many metastable states whose number scales as $e^{s_c(T)\xi^d}$, where s_c is the configurational entropy density which vanishes at the Kauzmann temperature, T_K.

(ii) The probability of finding a droplet in a given state i, given that its boundary conditions are in the state α is

$$p_{i\alpha} = \mathcal{Z}^{-1} e^{-\beta\left(\xi^d f_i + \xi^\theta \Upsilon_{i\alpha}\right)}, \tag{1}$$

where $\mathcal{Z}$ is a partition sum, f_i is the free energy density of state i and $\xi^\theta \Upsilon_{i\alpha}$ is the free energy cost of matching the bulk state i to the boundary state α. The exponent θ should satisfy $0 \leq \theta < d$ in a short ranged system.

(iii) Moves involving co-operative motion over a lengthscale ξ occur on a timescale

$$\tau \sim e^{\beta\Delta\xi^\psi}, \tag{2}$$

where Δ is a microscopic energy scale, and ψ is some exponent. If we assume that these moves involve nucleation events of one state in a background of an uncorrelated state then the exponent ψ is expected to obey $\psi \geq \theta$.

The lengthscale of the mosaic state can be extracted by comparing the probability of a droplet state satisfying a frozen boundary condition, with the total probability of all other droplet states with the same frozen boundary [18]. That is, choosing a state i such that $\Upsilon_{i\alpha} = 0$, we define the crossover length ξ_* by

$$e^{-\beta f_i \xi_*^d} = \sum_{j \neq i} e^{-\beta\left(\xi_*^d f_j + \xi_*^\theta \Upsilon_{j\alpha}\right)}. \tag{3}$$

The right hand side is a sum over $e^{s_c \xi_*^d}$ terms, so we can approximate it by

$$e^{-\beta f_i \xi_*^d} \simeq e^{-\left\{\xi_*^d [\beta f(T) - s_c(T)] + \xi_*^\theta \beta \Upsilon(T)\right\}}, \tag{4}$$

where the sum over states j was replaced with the typical number of terms in the sum, $e^{\xi^d s_c(T)}$, multiplied by the typical weight $e^{-\beta[\xi^d f(T) + \xi^\theta \Upsilon(T)]}$. We have included explicitly the temperature dependence of f, s_c and Υ, as they have been averaged over internal configurations of the droplet, subject to the boundary condition α. As long as the free energy of the well-matched state is typical, $f_i \simeq f(T)$, the mosaic lengthscale is

$$\xi_* \sim \left(\frac{\beta\Upsilon}{s_c}\right)^{\frac{1}{d-\theta}}. \tag{5}$$

The configurational energy of the droplet is thought to vanish at some finite T_K, which leads to the divergence of ξ_* at that temperature [2].

Combining these thermodynamical arguments, with assumption (iii) above we get the typical relaxation time for a droplet of size ξ_*,

$$\tau \sim \exp(\beta\Delta\xi_*^\psi). \tag{6}$$

Droplets of length smaller than ξ_* will not relax at all in this timescale. Droplets of length larger than ξ_* relax by combinations of moves over lengthscales of the order of ξ_* in times of the order of τ. Hence, τ gives the typical rate of rearrangements in the system [21].

B. Plaquette models

The BB procedure outlined in the previous subsection is extremely general. However, analysing the partition function of any model in sufficient detail to evaluate the length ξ_*, as defined in Eq. (3), is rather difficult. In the rest of this work we apply the procedure to two models of Ising spins with plaquette interactions in two dimensions.

We will define the models in the next section, but we first make some introductory remarks. The first model is the square plaquette model (SPM), in which spins are defined on a square lattice, and interactions involve the quartets of spins that form the square plaquettes of the lattice [14, 15]. In the second model, the spins occupy the sites of a triangular lattice, and interactions are between triplets of spins on upward pointing triangular plaquettes [16, 17]. We refer to it as the triangular plaquette model (TPM). Both models have dual representations [15, 17]:

in a spin representation they describe interacting spins with simple dynamical rules (single spin-flips); in a "defect" representation they describe thermodynamically independent excitations with more complicated dynamical rules. In this latter description they resemble the kinetically constrained models advocated as effective models for the glass transition in the dynamic facilitation approach [10]. In this sense, they interpolate between models with microscopic degrees of freedom, and more phenomenological models of "mobility fields".

The SPM and TPM have trivial thermodynamics: the excitations in the models are localized and statically non-interacting, so the only thermodynamic singularity is at zero temperature. In terms of our assumption (i), above, this means that we must have $T_K = 0$. It also has implications on the assumptions of (ii) and (iii) about the surface tension and barrier exponents θ and ψ. Below we show that the BB procedure can still be applied to extract caging lengthscales from finite-size static properties. However, while relaxation times grow with growing mosaic lengths, the quantitative dependence of assumption (iii) does not hold in the SPM and TPM, and these relations need to be generalized.

III. SQUARE PLAQUETTE MODEL

The SPM is defined by the Hamiltonian [14, 15]:

$$H = -(1/2)\sum_{xy}\left(\sigma_{xy}\sigma_{x,y+1}\sigma_{x+1,y}\sigma_{x+1,y+1} - 1\right), \quad (7)$$

where the $\{\sigma_{xy}\}$ are Ising spins, $\sigma = \pm 1$, and (x, y) indicates position on a square lattice. The dynamical moves are single spin-flips with Glauber rates. If we write

$$p_{xy} = \sigma_{xy}\sigma_{x,y+1}\sigma_{x+1,y}\sigma_{x+1,y+1}, \quad (8)$$

then the partition function is simply a sum over the non-interacting variables p_{xy} (up to a non-extensive set of constraints on the p_{xy} from the boundary conditions on the spins). The variables p_{xy} are defined on the plaquettes of the square lattice, which forms a dual square lattice, see Fig. 1. Plaquettes with $p_{xy} = -1$ cost an energy of unity, and are sparse at low temperatures: we refer to them as defects.

The plaquette model has activated dynamics at low temperatures. That is, there are very few (if any) possible transitions out of a typical state into states with lower energy. Thus, low temperature states are very close to inherent structures (on quenching to zero temperature, a few local relaxations will take place, quickly leading to a state with no available transitions). Thus it is an ideal model to investigate the mosaic hypothesis: there are many metastable states, and these can be easily identified. (In contrast, the statistics of the free energy minima of an atomistic liquid or a spin glass are much harder to probe).

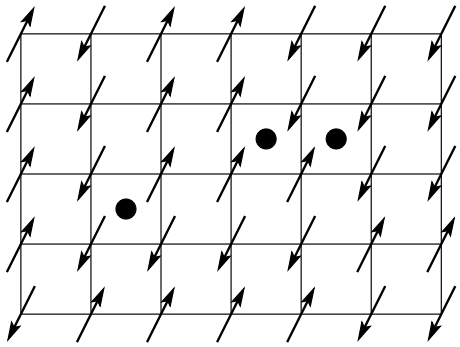

FIG. 1: Sketch showing spins (up or down) on vertices of a square lattice, and defect variables (circled or blank) on the dual lattice formed by the square plaquettes.

The trivial bulk thermodynamics of the SPM are affected by freezing the boundary spins of a finite droplet. Consider the partition function of a finite system of L^2 spins (assumed square for convenience), with $(4L-4)$ frozen spins along the boundary. The state of the system is then defined by the configuration of the $(L-2)^2$ remaining (bulk) spins, and its energy is given by (half of) the sum of the $(L-1)^2$ defect variables, p_{xy}. We see immediately that there are more configurations of the plaquettes than of the bulk spins: a partition sum over the bulk spins does not contain all configurations of the plaquette variables. Rather, there are

$$n_{\rm plaqs} - n_{\rm spins} = (L-1)^2 - (L-2)^2 = 2L - 3, \quad (9)$$

constraints on the possible arrangements of the defects.

To understand the origin of these constraints, observe that flipping any of the $(L-2)^2$ free spins preserves the parity of the number of defects in any row or column of the square (dual) lattice. Therefore the $2L-3$ constraints select the parity of the $L-1$ rows and $L-1$ columns of the dual lattice. [Fixing the parities of all the rows sets the parity of the total number of defects. Thus there are only $L-2$ independent column parities, the final one being fixed by the parity of the total number of defects. The result is that there are $2L-3$ independent constraints on the plaquettes, as required.] These arguments are illustrated in Fig. 2.

If we separate the energy of a configuration into a part coming from the $(L-3)^2$ plaquettes in the bulk, and the $4L-8$ plaquettes along the boundary then we may write the partition function for all L^2 spins as

$$\mathcal{Z} = \sum_{i\alpha} z_{i\alpha}, \qquad z_{i\alpha} \equiv e^{-\beta(n_i + n_{i\alpha})}, \quad (10)$$

where i labels the configuration of the bulk spins and α that of the boundary. The integer n_i is the number of bulk plaquettes that are excited, and $n_{i\alpha}$ is the number of boundary plaquettes that are excited. Making contact with section II, we identify n_i with the free energy f_i

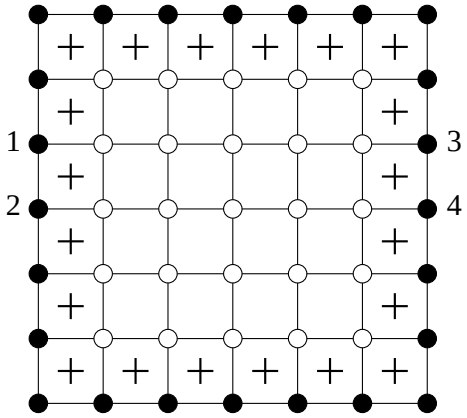

FIG. 2: A droplet of size $L = 7$. There are $(4L - 4) = 24$ frozen boundary spins (black circles) and $(L - 2)^2 = 25$ free bulk spins (white circles). The energy is determined by the state of the 36 defect variables that sit on the dual lattice. This energy can be divided into a boundary contribution that comes from the sites of the dual lattice marked with +, and a bulk contribution from the remaining sites. The partition sum is over the 2^{25} configurations of the bulk spins; these correspond to 2^{25} of the 2^{36} configurations of the defect variables. A given configuration of the defect variables contributes to the partition sum if and only if it satisfies the 9 independent constraints set by the frozen boundary spins. For example, one such constraint is that the parity of the number of defects in the third row of the dual lattice is the same as the frozen spin combination $\sigma_1\sigma_2\sigma_3\sigma_4$, where the spins σ_{1-4} are identified in the figure.

and $n_{i\alpha}$ with the surface energy $\Upsilon_{i\alpha}$. Note that we have replaced the sum in (3) over inherent structures by a sum over states, since the typical droplets under consideration cannot reduce their energy by any single spin-flip.

The partition function in (10) can be written in terms of partial sums over boundary conditions α,

$$\mathcal{Z} = \sum_\alpha Z_\alpha, \quad Z_\alpha \equiv \sum_i z_{i\alpha}. \tag{11}$$

Now imagine choosing a droplet in an infinite system. In doing so we find that its boundary state is α. The droplet lengthscale is calculated by considering the contribution of that droplet to Z_α. In other words, we need to estimate the expectation value of $z_{i\alpha}/Z_\alpha$ as a function of droplet size. This expectation value is

$$\left\langle \frac{z_{i\alpha}}{Z_\alpha} \right\rangle_L = \frac{1}{\mathcal{Z}} \sum_{i\alpha} \frac{z_{i\alpha}^2}{Z_\alpha} = \sum_\alpha \frac{Z_\alpha}{\mathcal{Z}} \sum_i \left(\frac{z_{i\alpha}}{Z_\alpha} \right)^2. \tag{12}$$

The second form for the expression above emphasises that it is an average over the boundary conditions with their thermal weights, Z_α.

We define ξ_* as the system size at which the above expectation value ceases to be dominated by a single state,

$$\langle z_{i\alpha}/Z_\alpha \rangle_{\xi_*} \equiv (1/2). \tag{13}$$

Since the droplet entropy is

$$S_\alpha = -k_B \sum_i (z_{i\alpha}/Z_\alpha) \log(z_{i\alpha}/Z_\alpha), \tag{14}$$

Eq. (13) will be satisfied when $\langle S_\alpha \rangle$ be of the order of k_B. In what follows we set $k_B = 1$. The entropy (14) measures the typical number of states contributing to the partition sum with a fixed boundary. It must not be confused with the configurational entropy which measures the number of states contributing to the overall partition sum.

A. Finite size thermodynamics

The partition function for a finite SPM with periodic boundaries was calculated by Espriu and Prats [22]. In appendix A we generalise their argument to allow for a given state of $4(L-1)$ fixed boundary spins. The derivation is in the spirit of a high temperature series, which can be resumed exactly for this model since the bulk thermodynamics are those of a trivial free lattice gas. As mentioned above, the boundary conditions on the spins constrain the parity of the number of defects in each row and column of the dual lattice. If the number of rows with odd parity is r and the number of columns with odd parity is r', then Z_α depends on the boundary conditions only through r and r'. Since it is a symmetric function of these two integers, it is convenient to define

$$m \equiv \max(r, r'), \qquad n \equiv |r - r'|, \tag{15}$$

so that $Z_\alpha = Z_{mn}$. Note that n is always even since r and r' (and therefore m) all have the parity of the total number of defects in the droplet. It is also convenient to parameterize temperature by:

$$c \equiv e^{-\beta}, \tag{16}$$

which is related to the average concentration of excitations by $\langle (1 - p_{xy})/2 \rangle = c/(1 + c) \approx c$, the last approximate equality being valid at low temperatures.

The low temperature behaviour of the plaquette model obeys scaling relations [23]. Length and timescales diverge at low temperatures as simple powers of c. We therefore work in the scaling regime, at leading order in c. In terms of droplet sizes, this means that numerical values of L may be large. The relevant indicators of droplet size will be cL and cL^2. That is, we assume $c \ll 1 \ll L$, but make no assumption on the absolute sizes of cL or cL^2.

We begin by considering fixed L and very low temperatures: $cL^2 \ll 1$. On picking a droplet from an infinite system, it is very likely that it contains no defects. The boundaries will then be such that all rows and columns contain even numbers of defects. There are 2^{2L-1} such boundary conditions (one for each choice of spins, say, in the bottom and leftmost sides of the box). Tracing over

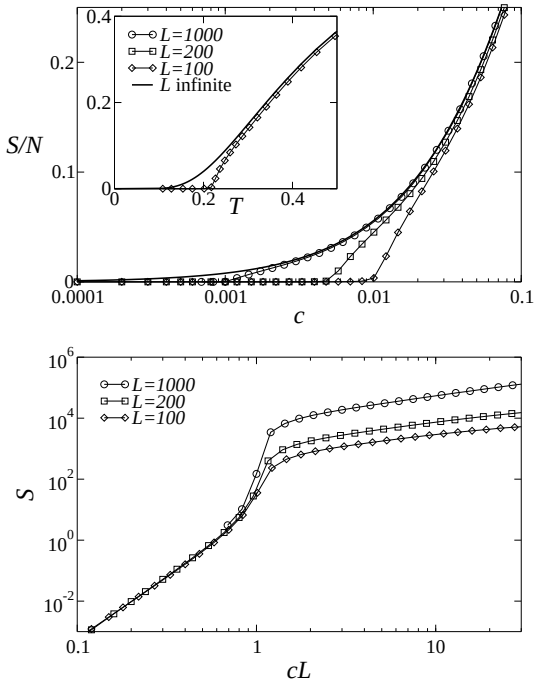

FIG. 3: (Top) Droplet entropy density S_{00}/L^2 versus $c \equiv e^{-\beta}$ for droplets of different sizes L, with frozen boundary conditions enforcing even numbers of defects in every row or column, $m = n = 0$. The symbols are finite L entropies calculated using the expressions of appendix A. The entropy is extensive for $cL > 1$. On approaching $cL \sim 1$ from above it deviates from the bulk entropy (solid line, $L \to \infty$), and becomes subextensive for $cL < 1$. (Bottom) Plot of total entropy S_{00} against cL showing the (non-extensive) scaling predicted in (18).

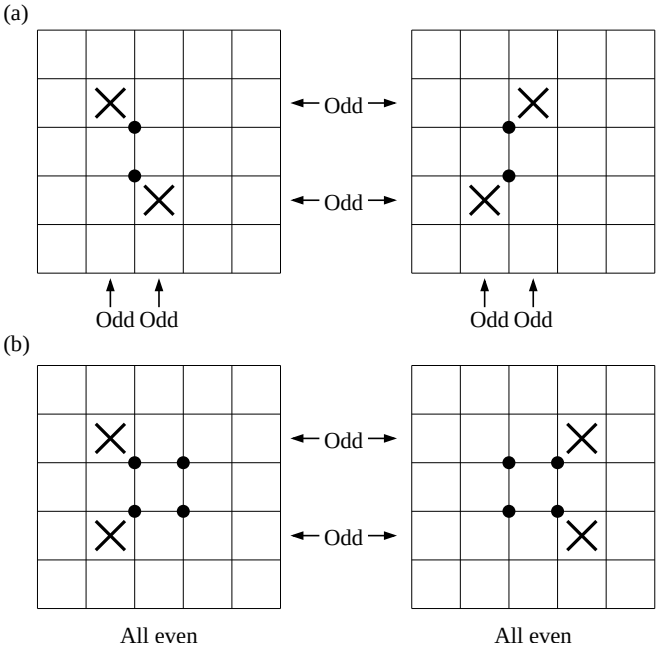

FIG. 4: Ground states of droplets ($L = 6$) with different boundary conditions. Spins are on vertices on the square lattice and are not shown. Excited plaquettes are marked with $\times$ symbols. (a) Boundary conditions enforce two rows and two columns with odd numbers of defects, so that $m = 2$, $n = 0$. There are two ground states that differ by flipping the two spins identified with black circles. (b) Boundary conditions enforce two rows with odd numbers of defects, but all columns with even numbers: $m = 2$, $n = 2$. There are $(L - 1) = 5$ distinct ground ground states of which two are shown: they differ only at the four marked spins

the bulk spins with each configuration of the boundary contributes $Z_\alpha = Z_{00} \equiv Z_{m=0,n=0}$ to $\mathcal{Z}$:

$$\mathcal{Z} = 2^{2L-1}[Z_{00} + \mathcal{O}(cL^2)]. \tag{17}$$

Now, if $m = n = 0$ then the boundary of the droplet specifies its unique ground state. Further, simple counting arguments show that excited states contain even numbers of defects $u \geq 4$. Their Boltzmann weights are c^u and the degeneracy of the state with u defects is proportional to L^u. This means that:

$$Z_{00} = 1 + \mathcal{O}(cL). \tag{18}$$

This partition function is also relevant to periodic boundary conditions, and is the one calculated in [22]. In Fig. 3 we show the droplet entropy $S_{00} = \partial_T(T \ln Z_{00})$, as a function of c for different droplet sizes L. The top panel of Fig. 3 shows that the droplet has an "entropy crisis" at $cL \sim 1$. In the bottom panel of Fig. 3 we see that the droplet entropy scales with cL when $cL \ll 1$, and is subextensive in this regime.

From figure 3, it is clear that as the temperature is increased, droplets with $m = n = 0$ remain frozen until $cL \sim 1$. However, Z_{00} dominates the droplet partition function only for $cL^2 \ll 1$. This means that *typical* droplets are frozen only for $cL^2 \ll 1$. Between $cL \sim 1$ and $cL^2 \sim 1$ we must consider Z_{mn} with $m, n \neq 0$.

The behaviour of droplets changes qualitatively in the case of ground states containing two or more defects. As is clear from Fig. 4, if $m \geq 2$ then there is more than one state of the bulk spins that satisfies the boundary condition perfectly. Specifically, if $m = 2$ then there are two ground states, each of which contains two defects, and contributes c^2 to the partition function. More generally, we find that

$$Z_{m0} \sim m!\, c^m[1 + \mathcal{O}(cL)]. \tag{19}$$

It follows that the zero temperature droplet entropy is now $S_{m0}(T = 0) = \log m!$, and so for these boundary states, we expect typical values of

$$z_{i\alpha}/Z_\alpha \sim (1/m!) + \mathcal{O}(cL). \tag{20}$$

While the droplets do have a feature in the entropy at $cL \sim 1$, the degenerate ground states all contribute equally to the partition sum at low temperature. Thus, as soon as droplets with $m \geq 2$ dominate $\mathcal{Z}$ then the

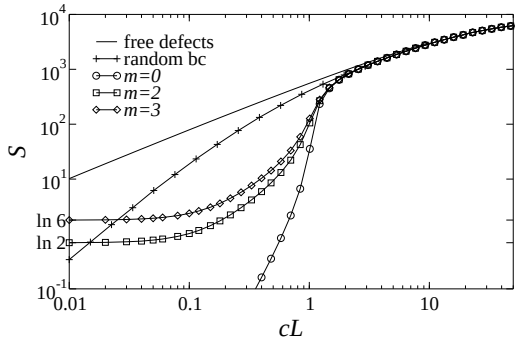

FIG. 5: Entropy as a function of cL for $L = 100$. The full line is the bulk entropy of the SPM. The open symbols are the entropies S_{m0} for frozen boundaries with different m, as obtained from the finite size partition functions of appendix A. The + symbols give the entropy in the case where boundary conditions are generated randomly.

they are thermodynamically melted according to condition (13). Fig. 5 shows that this happens as soon as $cL^2 \sim 1$, as expected. The melting lengthscale is therefore,

$$\xi_* \sim c^{-1/2}. \tag{21}$$

It is clear that there are two crossovers in the droplet thermodynamics as c is increased. For $cL^2 \ll 1$ nearly all droplets are frozen in true ground states of the system. For $cL \gg 1$ the system behaves as the bulk. In the intermediate regime $cL \ll 1 \ll cL^2$, each droplet is almost certainly in a state that minimises the energy with respect to the boundaries; however, there are many of these states for a fixed configuration of the boundary. In this regime m is about cL^2. The low temperature droplet entropy is then

$$S_{T=0} \simeq cL^2 \log cL^2, \tag{22}$$

which is large compared to unity, but small compared to its bulk value $cL^2 \log 1/c$ (since $cL \ll 1$ implies $cL^2 \ll 1/c$). We show this explicitly in Fig. 5 where we average the exact results for the entropy at given m and n over a distribution of mn that is sampled by Monte Carlo.

Thus far we have analyzed only states with $n = 0$. That is, the boundary condition requires m rows to have odd numbers of defects in them, and it also requires m columns to have the same property. The probability that $n = 0$ is the probability that no two defects occupy the same row or columns as each other,

$$P(n = 0) = 1 - \mathcal{O}(c^2 L^3). \tag{23}$$

This probability is close to 1 as long as $cL^2 \ll \sqrt{L}$.

The melting length (21) can also be accessed through static overlap functions, which will be important in our discussion of dynamics. Consider the self-overlap for a given boundary α,

$$C_{0\alpha} = \frac{1}{(L-2)^2} \sum_{xy} \langle \sigma_{xy} \rangle_\alpha^2 \,, \tag{24}$$

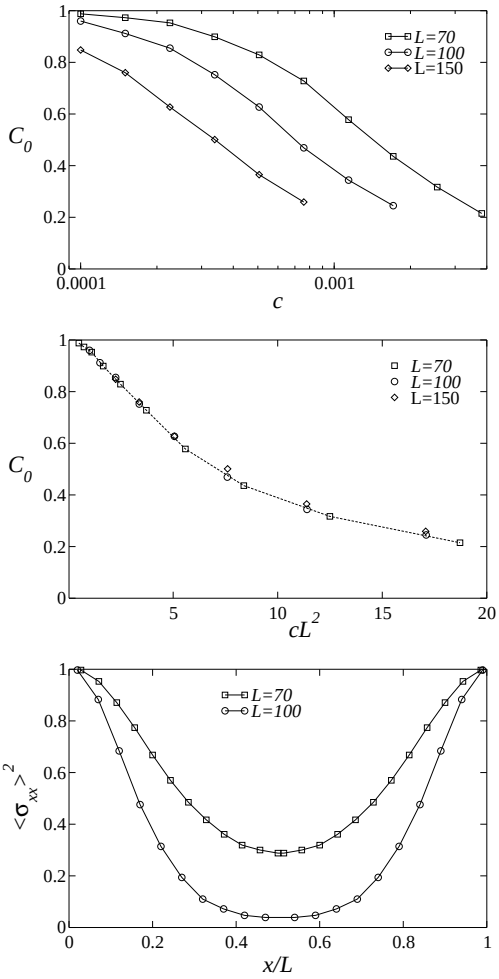

FIG. 6: Plots of the overlap function $\langle \sigma_{xy} \rangle_\alpha^2$, averaged over boundary conditions α at various temperatures. (Top) Average overlap C_0 as a function of temperature. (Middle) Collapse of this data as a function of cL^2 (the dashed line is a guide to the eye). (Bottom) Spatial dependence along the diagonal of the square droplet, showing strong correlations near the boundary.

where we have explicitly summed over the spins of a droplet with given boundary condition, since for a given realisation of the α, single spin correlations are finite and depend on position. The brackets $\langle \ldots \rangle_\alpha$ denote a thermal average over configurations of the bulk spins, with the boundary spins fixed. $C_{0\alpha}$ should give the long time limit of the spin-spin autocorrelation for a droplet with given boundary conditions. Averaging over the boundary spins we get:

$$C_0 = \sum_\alpha Z_\alpha C_{0\alpha}, \tag{25}$$

which is analogous to a disorder average.

In Fig. 6 we show these overlaps. The correlator $\langle \sigma_{xy} \rangle_\alpha$ can be calculated in a high temperature series: see appendix A. The top and middle panels of Fig. 6 show

that C_0 is a function of cL^2, which is close to 1 for small cL^2, and becomes small when cL^2 gets large. This scaling also indicates that C_0 will be small in the regime $cL \ll 1 \ll cL^2$. The bottom panel of Fig. 6 shows the spatial dependence of $\langle \sigma_{xy} \rangle_\alpha$. The spins near the boundaries are strongly fixed by the boundary condition. This correlation decays away from the boundary with a lengthscale that scales as $\xi_4 \sim c^{-1/2}$. These observations for the overlaps are consistent with thermodynamic melting of the droplet at $cL^2 \sim 1$ found above.

B. SPM and mosaic lengths

We have established that the melting lengthscale ξ^* scales as $c^{-1/2}$ in the SPM, but that there is also a second important thermodynamic crossover at $L \sim c^{-1} > \xi_*$. We now compare the results so far with the expectations of BB. The appearance of two lengthscales was not anticipated in [18]. We have shown that the crossover at $cL^2 \sim 1$ comes from a small number of states that are have similar weights in the droplet partition function. We find that distinguishing these few specific states from typical states with bulk energy E is necessary when discussing the droplet partition function Z_α.

We use (3) to define the mosaic lengthscale ξ_*. The assumption of BB is that the lengthscale defined by (4) will scale in a similar way. Eq. (3) treats all states individually, whereas (4) assumes that we can extrapolate the properties of the partition sum from typical states at the relevant temperature. We write the mosaic lengthscale extracted from (4) as $\xi_{*,\mathrm{typ}}$: we find that ξ_* and $\xi_{*,\mathrm{typ}}$ do not coincide in the SPM.

More precisely, the average bulk energy of a droplet at a given temperature is $c(L-2)^2$, and the configurational entropy at that temperature is $c(L-2)^2 \ln(1/c) + (2L-1)\ln 2$. If we replace the bulk of the droplet by a new bulk state with the same energy, then the typical boundary energy is $2(L-2)$ (half of the boundary plaquettes will be excited, since there are no two-point spin correlations either in the bulk or along the boundary). So from Eq. (4), we have $d = 2$, $\theta = 1$ and

$$\xi_{*,\mathrm{typ}} \sim c^{-1}$$

On the other hand, we showed in the previous section that the Eq. (3) leads to

$$\xi_* \sim c^{-1/2}$$

The origin of this discrepancy is simply the degenerate ground states of the droplet, whose boundary energy does not take the typical value $\Upsilon(T) \sim L$, but rather have $\Upsilon_{i\alpha} = 0$. Thus they must be separated from the sum before it is approximated:

$$Z_\alpha = e^{-\beta f_i L^2} + \sum_{j \neq i, j \in \mathrm{gs}} e^{-\beta f_j L^2} + \sum_{j \neq i, j \notin \mathrm{gs}} e^{-\beta f_j L^2 - \beta \Upsilon_{j\alpha}} \quad (26)$$

where the sum over $j \in$ gs denotes a sum over states with $\Upsilon_{j\alpha} = 0$. The final term in (26) can then be approximated to give a form resembling Eq. (4), but that term is irrelevant to droplet melting in the SPM since the second term dominates the partition sum for $cL \ll 1 \ll cL^2$.

We interpret this result as evidence that approximations such as those leading to Eq. (4) are rather dangerous. In general, systems may possess significant numbers of states in the partition sum with smaller than average boundary energy, and these may be sufficient to destroy spin correlations in the infinite time limit ($C_0 \to 0$ when $L \ll \xi_{*,\mathrm{typ}}$), even if the droplet is exploring only a small fraction of its metastable states. Further, we will show in the next section that if the droplet does melt in stages then choosing whether to identify the bulk relaxation time as $\tau(\xi_*)$ or $\tau(\xi_{*,\mathrm{typ}})$ requires investigation of the specific system under study. In the SPM, we will find that while complete destruction of of spin correlations at large times does take place for $L \ll \xi_{*,\mathrm{typ}}$, the timescale for this relaxation is much longer than the bulk relaxation time. However, this effect cannot be inferred from thermodynamic arguments: it is a kinetic effect.

To end this discussion, we note that while the condition $cL^2 \sim 1$ leads to rather small droplets, the configurational entropy of a droplet of this size is $cL^2 \log(1/c) \gg 1$. BB comment that the vanishing of the configurational entropy leads to a trivial lower bound on the mosaic lengthscale which in this case is: $\xi_*^2 > [c \log(1/c)]^{-1}$. Thus we see that despite the condition that frozen droplets contain at most one defect, the freezing lengthscale is still much larger than its trivial lower bound.

C. Relaxational dynamics

In this subsection we consider the relaxation of the droplets studied thermodynamically above. The relevant correlation function is

$$C_\alpha(t) = \frac{1}{(L-2)^2} \sum_{xy \in \mathrm{bulk}} \langle \sigma_{xy}(0) \sigma_{xy}(t) \rangle_\alpha \quad (27)$$

where the average is over realisations of the Markov chain that describes the time evolution of steady state of the system (with fixed boundary state α). We also define the average of $C_\alpha(t)$ over boundary conditions

$$C(t) = \sum_\alpha Z_\alpha C_\alpha(t) \quad (28)$$

The long time limit of $c_\alpha(t)$ is given by the overlap $c_{0\alpha}$.

¿From Monte Carlo simulations, it is clear that the relaxation of the system slows down as the system size is decreased towards $1/c$: see Fig. 7. From our discussions of the static single point correlator [Eq. (24) and Fig. 6] we expect the long time limit of this function to approach zero even for $cL \ll 1 \ll cL^2$, although this is hard to show in simulations since simulations with large numbers

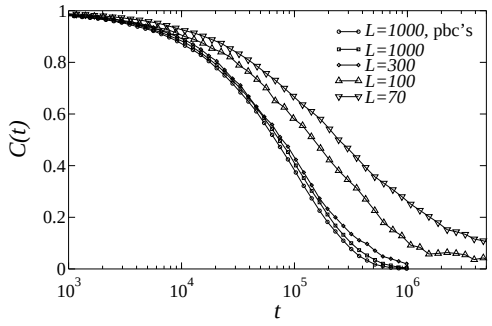

FIG. 7: Simulations of the SPM at $c = 0.01$ for various system sizes and frozen boundary conditions. The relaxation time increases significantly as cL decreases through unity, but the long time limit of $C(t)$ would still appear to vanish since $cL^2 \gg 1$. We also show relaxation for $L = 1000$ and periodic boundary conditions. The relaxation can be well-fitted by an exponential for large L. At smaller L the decay is slower than exponential.

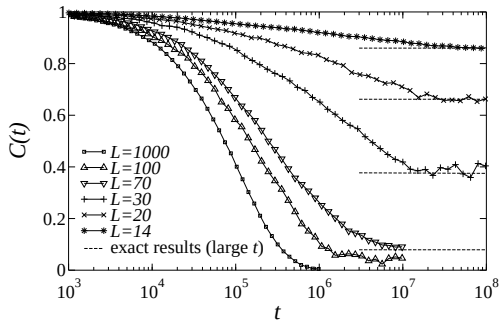

FIG. 8: Simulations of the SPM at $c = 0.01$ for various system sizes and frozen boundary conditions. The long time limit of $C(t)$ increases from zero as cL^2 becomes of order unity.

of defects at small temperatures are very computationally expensive.

Moving towards the regime with $cL^2 \sim 1$, we see that the relaxation of the system is very slow, and that there are large correlations that persist to the infinite time limit: see Fig. 8. We can make a link between static and dynamic quantities by evaluation of the long time limit of these functions using the high temperature series (cf. Fig. 6).

Thus we have shown how the two lengthscales associated with the glassy mosaic state affect the dynamics of the system. As the temperature is reduced, the relaxation slows for $cL \sim 1$, before stopping completely at $cL^2 \sim 1$. The separation of these lengthscales was not anticipated in [18]: we have more to say on this below.

Before ending our discussion of dynamics, we make two further points. Firstly, we note that it is clear from Ref. [23] that the bulk relaxation is caused by correlated motion of defects over distances $\xi_{\rm dyn} \sim c^{-1}$. This coincides with the system size above which the system relaxes as the bulk. Secondly, it is also known [22, 23] that correlated motion for defects over a distance l takes place on a timescale $\tau \sim le^{2\beta}$ so we see that the analogue for equation (2) is

$$\tau \sim e^{2\beta + \log \xi} \tag{29}$$

The exponent depends logarithmically on ξ with a prefactor that does not depend on temperature: apart from the constant activation energy, the free energy barriers to motion are purely entropic in origin. The entropic nature of the barriers explains why relaxation of the SPM model diverges only in an Arrhenius fashion ($\tau \sim e^{3\beta}$) despite the co-operativity of its dynamics.

D. SPM summary

It is clear from the results of this section that, even in a simple model like the SPM, the situation regarding caging and mosaic lengthscales is already more complicated than what the appealingly simple and general arguments of [18] would predict. As we increase the size of droplets with frozen boundaries, there are two crossovers. Static spin-spin correlations vanish at at $c \sim L^{-2}$, but neither the droplet entropy, nor its dynamical correlation functions reach their bulk forms until the much higher temperature $c \sim L^{-1}$. We note that these two lengthscales were also identified in the discussion of static and dynamic lengthscales in Ref. [23]. To be precise, the static four-spin correlator $\langle \sigma_{00}\sigma_{0r}\sigma_{r0}\sigma_{rr}\rangle$ decays on a lengthscale $\xi_4^{\rm stat} \sim c^{-1/2}$, but the dynamic four point correlator decays on a length that scales as $\xi_{2,2} \sim c^{-1}$. There is also a static lengthscale that mirrors the scaling of $\xi_{2,2}$ which is derived from fluctuations of two point correlations [23].

Despite these complications, a general picture like that of [18] does seem to be applicable to the SPM, in the sense that droplet melting does occur, even if it happens in stages. As the temperature decreases towards the Kauzmann singularity at $T = 0$, the mosaic lengthscale increases, and the relaxation time increases according to (29). This increase follows a simple Arrhenius law because only the entropic barriers depend on ξ_*. This suggests that one should replace (2) by the more general parametrization

$$\tau \sim f_s(\xi) e^{\beta f_u(\xi)} \tag{30}$$

where $f_s(\xi)$ describes the entropic part of the barrier and $f_u(\xi)$ the energetic part. At small temperatures then we expect the energetic part to dominate, except in the case where $f_u(\xi)$ is independent of ξ, as is the case for the SPM.

It is at this point at which our discussion of dynamics diverges from that of KTW and BB: since the (non-perturbative) dynamical moves are not nucleation events in this model, then the free energy barrier is not set by a transition state with a critical droplet of the new phase.

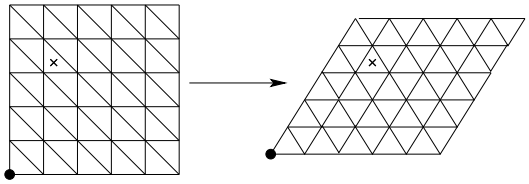

FIG. 9: Sketch showing relation between square and rhomboid droplets ($L = 6$). The spins are on the intersections of grids; σ_{11} is marked by a filled circle. The $\times$ symbol marks the plaquette interaction $q_{24} = \sigma_{24}\sigma_{25}\sigma_{34}$. Rotations of 120° leave both Hamiltonian and triangular lattices invariant. However, note that the boundaries of the droplets are not all equivalent, since the rhombus shape is not invariant under this rotation.

Rather, the relaxation proceeds by less expensive rearrangements that occur over a lengthscale $\xi_{*,\mathrm{typ}}$, as was discussed in detail in Ref.[23].

IV. TRIANGULAR PLAQUETTE MODEL

In this section we compare the results we found above for the SPM, with a similar model of Ising spins: the triangular plaquette model, or TPM [16, 17]. This model has a super-Arrhenius divergence of the relaxation time at low temperatures, and is therefore a fragile model, as compared to the SPM, which is strong. Moreover, dynamical correlations do not have the strong anisotropy of the SPM [23]. The calculation of the partition function, however, is considerably more involved, so our results below are less detailed than those for the SPM.

The TPM is defined by the Hamiltonian [16, 17]:

$$H = -(1/2)\sum_{xy} \sigma_{xy}\sigma_{x+1,y}\sigma_{x,y+1}. \tag{31}$$

where as before $\{\sigma_{xy}\}$ are Ising spins on a square lattice and the dynamics are is spin-flips with Glauber rates. If we define the plaquette variables

$$q_{xy} = \sigma_{xy}\sigma_{x+1,y}\sigma_{x,y+1} \tag{32}$$

we again find that the partition sum over the spins reduces to a product over q_{xy}, that are independent up to a non-extensive set of constraints from the boundary conditions [15, 16].

We note that defining this model in this way leads to a Hamiltonian that does not possess the square symmetry group of the lattice: it is more intuitive to deform the square lattice into a triangular one. The interactions are then around upward pointing triangular plaquettes (see Fig. 9). The symmetries of the Hamiltonian are then translations by lattice vectors, and 120° rotations (60° rotations leave the lattice invariant but flip downward pointing triangles to upward pointing ones, so they change the Hamiltonian).

The analogy of the square droplet of Fig. 1 is a rhombus shape in the triangular representation. The arguments for counting bulk and boundary states are the same as those of the plaquette model. However, identifying the 2^{2L-1} degeneracies of each state and the nature of the $(2L-3)$ constraints is considerably more involved.

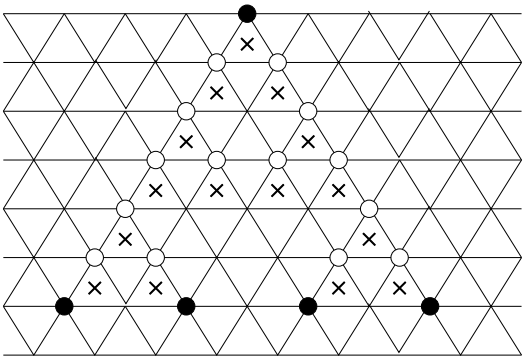

FIG. 10: Illustration of Eq. (36) with $k = 6$. The product of the five spins marked by filled circles is given by the product of the fifteen plaquette variables marked with crosses. Both the marked defects and the spins marked with circles (filled *and* empty) form parts of Sierpinski triangles: they are marked if and only if the relevant entry of Pascal's triangle is odd.

A. Static spin-spin correlations and constraints

The key to understanding static properties of the triangular plaquette model is to realise that

$$\langle q_{i_1,j_1} q_{i_2,j_2} \dots q_{i_n,j_n} \rangle = [\tanh(\beta/2)]^n. \tag{33}$$

All multi-spin correlators that can be written in this form are finite. Further, all other multi-spin correlators are zero [15]. While one and two point static spin correlations vanish,

$$\langle \sigma_{xy} \rangle = 0, \quad \langle \sigma_{xy}\sigma_{x'y'} \rangle = \delta_{x,x'}\delta_{y,y'}, \tag{34}$$

specific three point correlators are non-zero,

$$\langle \sigma_{xy}\sigma_{x+1,y}\sigma_{x,y+1} \rangle = \langle q_{xy} \rangle = \tanh(\beta/2). \tag{35}$$

A useful general relation is that

$$\sigma_{xy} \prod_{r=0}^{k} \sigma_{x+r,y-k}^{B_{k,r}} = \prod_{k'=1}^{k} \prod_{r=0}^{k'-1} q_{x+r,y-k'}^{B_{k',r'}}, \tag{36}$$

where the $B_{nr} \equiv n!/[r!(n-r)!]$ are binomial coefficients. Since the q's and the σ's are Ising variables, only the parities of the binomial coefficients are relevant. In terms of correlation functions, this relation implies that there is a finite multi-spin correlator connecting σ_{xy} and various spins in row $x-k$ of the lattice.

This correlator is related to the first k rows of Pascal's triangle (PT). The correlator connects the spins corresponding to entries of the kth row of the PT that have odd parity. Its value is given by $\tanh(\beta/2)^p$ where p is

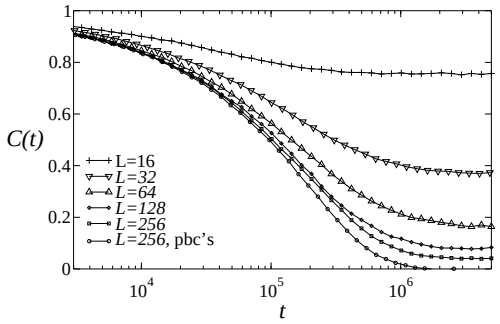

FIG. 11: Relaxation of finite systems at inverse temperature $\beta = 4$ ($c = 0.018$). Notice that the long-time limit of $C(t)$ is changing, but that the relaxation time is approximately constant. Compare to Fig. 8, where the relaxation time increases sharply as $C(t \to \infty)$ increases.

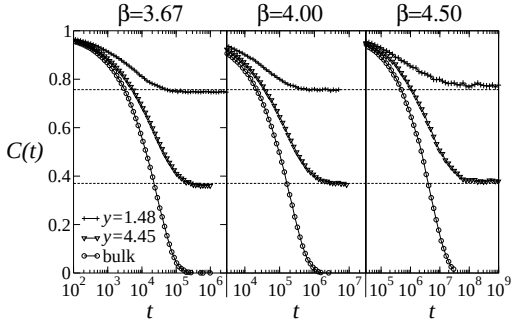

FIG. 12: Relaxation at different temperatures showing bulk results (circles) and two different values of cL^{d_f}. The actual system sizes used are (left) $L = 13, 26$; (middle) $L = 16, 32$; (right) $L = 26, 44$. The dashed lines are guides to the eye showing that the long time limit scales as a function of cL^{d_f} only (there are weak deviations from scaling which we attribute to subleading corrections in c and $1/L$).

the number of entries in the first $k-1$ rows of the PT that have odd parity. See Fig. 10 and the associated caption. Now, the typical number of odd entries in a Pascal's triangle of linear size l is l^{d_f} with $d_f = \log_2(3)$. It follows that typical correlations over a lengthscale r scale as

$$\tanh(\beta/2)^{(r^{d_f})} \sim \exp\left[-2(rc^{1/d_f})^{d_f}\right], \qquad (37)$$

from which we infer that static correlations decay on a lengthscale

$$\xi_{\rm stat} \sim c^{-1/d_f}. \qquad (38)$$

In the case of finite droplets there must be $(2L-1)$ symmetry operations that leave the energy of a droplet invariant, but require the boundary spins to change (recall Fig. 2). Furthermore, fixing the boundary spins imposes $(2L-3)$ constraints on the allowed configurations of the plaquette variables. The form of these symmetries and constraints are given explicitly in appendix B.

The SPM was simple to analyse since the constraints are in a form where each plaquette appears in exactly two constraints. In that case we can make a geometrical interpretation of those constraints. In the TPM the consequences of imposing the constraints is less clear. We therefore proceed directly to a discussion of dynamic properties, in an attempt to access the static properties indirectly.

B. Dynamic spin correlations

Relaxation in the TPM is frustrated by a hierarchy of energy barriers[16, 17]: co-operative motion over a distance ξ requires the crossing of an energy barrier of a height $\log_2 \xi$. This behaviour is reminiscent of the East model [12].

In order to understand the scaling of the mosaic length, we investigate the scaling of $C(t)$ in finite droplets: see figure 11. A lower bound on the freezing lengthscale is set by the elementary condition $cL^2 \sim 1$, since all states with single defects have different boundary conditions. This would imply that the long time limit of the autocorrelation, C_0 should be a scaling function of cL^2, as in the SPM, Fig. 6.

However, from the discussions of static correlations above, it is clear that the physics of the triangular plaquette model is intrinsically related to the parities of binomial co-efficients, and hence to Sierpinski's triangle. As mentioned above, this structure has a fractal dimension of $d_f = \log_2(3) \simeq 1.585$. In Fig. 12 we show relaxation data at various temperatures with constant values of cL^{d_f}. We see that C_0 does seem to depend only on this combination. The conclusion is that the mosaic lengthscale scales as

$$\xi_* \sim c^{-1/d_f}. \qquad (39)$$

This relation indicates that typical droplets melt when they contain of the order of $c^{1-2/d_f} \sim c^{-0.26}$ defects; below this number there no co-operative mechanisms allowing the droplet to rearrange. This should be compared with the SPM, in which droplets with $L \sim \xi_*$ contain of the order of one defect, but those at the dynamical crossover ($cL \sim 1$) contain of the order of c^{-1} defects.

An alternative measure of the co-operativity of the dynamics is given by the bulk "four-point" correlation function (see e.g. [24])

$$\tilde{G}_4(xy;t) = \langle \sigma_{xy}(t)\sigma_{00}(t)\sigma_{xy}(0)\sigma_{00}(t)\rangle. \qquad (40)$$

This correlation function measures spatial correlations in the single site autocorrelation function. It is convenient here to work with the connected part of this function, normalised according to

$$G_4(xy;t) = \frac{\tilde{G}_4(xy;t) - \langle \sigma_{00}(t)\sigma_{00}(0)\rangle^2}{1 - \langle \sigma_{00}(t)\sigma_{00}(0)\rangle^2}. \qquad (41)$$

In the triangular plaquette model, the function G_4 has a complicated spatio-temporal structure, again related to

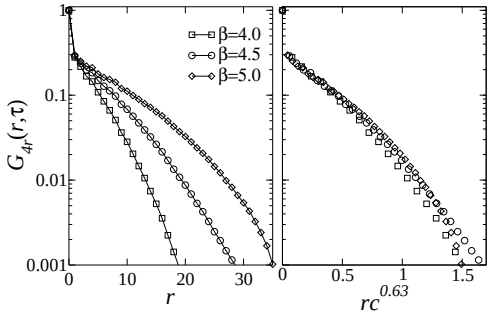

FIG. 13: Circular average of the normalised four point dynamic correlator. The system size is $L = 128$ with periodic boundaries, which is large enough to avoid finite size effects. (Left panel) Three different temperatures, with times chosen so that $C(t) = 0.5$. (Right panel) Collapse of the data of the left panel on rescaling of length as rc^{1/d_f}.

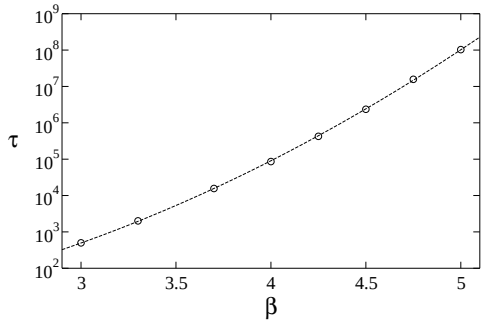

FIG. 14: Data showing relaxation time for large systems as a function of inverse temperature, β. The relaxation time is defined by $C(\tau) = 0.5$. The error bars are smaller than the symbols shown. The dashed line is a fit to the form $\ln \tau = a_0 + a_1\beta + q\beta^2/\ln 3$. Good fits are also possible with different coefficients for the quadratic term.

Sierpinski's triangle: we postpone a detailed discussion of this structure to a later work. However, the circular average of this function, which we denote by $G_{4r}(r,t)$ decays smoothly with distance (at a fixed time). This is shown in Fig. 13, from which it is clear that the lengthscale over which dynamical correlations occur also scales as

$$\xi_{\rm dyn} \sim c^{-1/d_f}. \tag{42}$$

We have used the dynamics of finite droplets to identify a single mosaic lengthscale in the triangular plaquette model, that scales as c^{-1/d_f}. Further, we know [17] that energy barriers to motion over a lengthscale l require an activation energy of the order of $\log_2 l$. At very low temperatures, we therefore expect the bulk relaxation time at very low temperatures to scale as

$$\tau \sim \exp\left(\beta \log_2 \xi\right) \sim \exp\left(\beta^2/\ln 3\right). \tag{43}$$

Note that Ref. [15] predicted $\exp(\beta^2/\ln 4)$ based on the assumption that $\xi \sim c^{1/2}$. Fig. 14 shows a fit of the relaxation time of $C(t)$ with the function $\ln\tau = a_0 + a_1\beta + \beta^2/\ln 3$. The constant and linear terms come from entropic and dynamical effects which become irrelevant at very low temperatures where the energy barriers on ξ dominate, see Eq. (30). The fit in the figure is consistent with (43), although the range of β that we consider is too small to confirm it beyond doubt.

C. TPM summary

The thermodynamics of finite droplets in the triangular plaquette model are not sufficiently simple to allow an analysis of the droplet entropy and hence determination of the mosaic lengthscale according to the criterion (3). However, it appears that the long time limit of the single spin autocorrelation function approaches unity as $cL^{\log_2 3}$ gets small. If C_0 approaches unity then it seems reasonable to assume that droplets are effectively trapped in a single state that dominates the partition sum, and that this should be an equivalent criterion to (3).

We find that the mosaic lengthscale extracted in this way (ξ_*), scales in the same way as the static lengthscale for multi-spin correlations ($\xi_{\rm stat}$), and as the dynamical lengthscale extracted from the four point correlator ($\xi_{\rm dyn}$). This scaling is evidence for the presence of a single lengthscale in this model. This is in contrast to the TPM, and more in line with [18].

On the relation of dynamics to statics, the analogue of (2) seems to be

$$\tau \sim f_s(\xi) e^{\beta \log_2 \xi} \tag{44}$$

The increase of the energy barriers with ξ is again slower than the power law predicted by [18], but the assumption of an increasing function is robust. The absence of a power law dependence again indicates that the system relaxes by a more efficient mechanism than nucleation of a new droplet in the background of an uncorrelated state.

V. CONCLUSIONS

We have successfully applied the procedure of Ref. [18] to two simple models of interacting Ising spins. We find that the concept of "caging" whereby the states of individual spins are strongly constrained by frozen spins surrounding them applies well in these models. We were able to study the breakdown of this caging effect by considering droplets of increasing size.

In the square plaquette model (SPM), the caging breaks down in two stages as the droplet size increases. For $L \ll c^{-1/2}$ the droplet is frozen. For $c^{-1/2} \ll L \ll c^{-1}$ the droplet will eventually relax, but this relaxation is slower than that of the bulk system. Finally, for $L \gg c^{-1}$ the relaxation time coincides with that of the bulk. The correlation lengths controlling these two

crossovers have the same scalings as the two separate lengths identified in this model from four point static and dynamic correlations[23]. The two stage droplet melting in this model is more complicated than the simple scenario of BB. Interestingly, the two crossover temperatures of the SPM, as well as the structure of the droplet states in the intermediate regime, bear some resemblance with the situation in mean-field systems like the p-spin model (see e.g. [25] and references therein).

In the triangular plaquette model (TPM) we find only a single crossover in the system at $L \sim c^{-1/\log_2 3}$. This is more in line with the situation anticipated in BB. The same lengthscale is again present in static multi-spin correlation functions, and in four-point dynamical correlators.

We draw two conclusions from these results. Firstly, we are able to verify that the procedure of BB is a suitable way to identify a mosaic lengthscale. In the general case it may be difficult to test the criterion (3) directly, although it is possible in the SPM. In less favourable situations, it is still possible to use dynamical studies to extract the mosaic lengthscale, as we showed for the TPM.

Secondly, we have shown that models without a finite temperature phase transition can still be described from the mosaic perspective of KTW and BB. This indicates that the concept of a glassy mosaic state is more general than the specific picture of KTW. While the low temperature states of the plaquette models are constructed by tiling the plane with different metastable configurations of the spin system, there are no well-defined droplets or domain walls in these states. Rather, there are point-like defects that allow the system to interpolate smoothly between different metastable configurations. The crucial difference with the KTW approach is that, while dynamics does proceed by non-perturbative events that require co-operation over a lengthscale that diverges at low temperatures, these events are not related to nucleation, but to more efficient rearrangements of the point-like defects.

In summary, typical states in the plaquette models are glassy mosaics whose dynamics should be understood in terms of point defects with co-operative dynamical rules. These defects are not locally conserved, and are not related to any concept of free volume. Rather, they represent regions in which the free energy barriers to motion are smaller than average. In this approach, the "activated processes" that dominate glassy α-relaxation involve co-operative rearrangements of defects over a lengthscale ξ. The time scales for these processes increase with ξ, with a general relation similar to (30).

The purpose of this work has been to investigate rather general arguments of KTW and BB explicitly in specific, and rather simple, finite dimensional models. We find good evidence for a generalised caging effect, but our view of static and dynamic properties of the glassy mosaic is qualitatively different from that of KTW. The possible links between spatial variation in the mosaic length and dynamical heterogeneity remain as an area for further study.

Acknowledgments

We thank G. Biroli and D. Sherrington for discussions. This work was supported by EPSRC grants no. GR/R83712/01 and GR/S54074/01, and University of Nottingham grant no. FEF 3024.

APPENDIX A: HIGH TEMPERATURE SERIES IN THE SPM

We follow [22] in making a high temperature expansion for the square plaquette model. The partition function for a droplet of size L with fixed boundary spins is

$$Z_\alpha = e^{-(L-1)^2\beta/2} \sum_{\text{bulk } \sigma_{xy}} \prod_{1\le xy\le L-1} e^{-\beta p_{xy}/2}, \quad \text{(A1)}$$

with

$$p_{xy} = \sigma_{xy}\sigma_{x+1,y}\sigma_{x,y+1}\sigma_{x+1,y+1}, \quad \text{(A2)}$$

as above. Since the p_{xy} are Ising variables then this can be written

$$Z_\alpha = \left(\frac{1+c}{2}\right)^{(L-1)^2} \sum_{\text{bulk } \sigma_{xy}} \prod_{1\le xy\le L-1} (1+zp_{xy}), \quad \text{(A3)}$$

where $z = \tanh(\beta/2) = (1-c)/(1+c)$.

Expanding the product results in a power series in z: there are $2^{(L-1)^2}$ terms corresponding to states of a dual system where the spins are the p_{xy}. Each state is equal to a power of z multiplied by a combination of the σ_{xy}; the term vanishes on summation over the σ_{xy} if it contains any spin to an odd power. Otherwise, the coefficient of the power of z depends only on boundary spins: in that case, the sum over bulk spins just contributes a trivial factor $2^{(L-2)^2}$.

Terms containing bulk spins to even powers are formed by flipping whole rows and columns of the dual p_{xy} variables. The result is that

$$\begin{aligned} Z_\alpha \;=\; & 2^{-2L+3}(1+c)^{(L-1)^2}(1/2)\times \\ & \sum_{h_y,v_x\in\{0,1\}} z^{(H+V)(L-1)-2HV}\times \\ & \prod_{1\le y\le L-1} \left(\sigma_{1y}\sigma_{1,y+1}\sigma_{Ly}\sigma_{L,y+1}\right)^{h_y}\times \\ & \prod_{1\le x\le L-1} \left(\sigma_{x1}\sigma_{x+1,1}\sigma_{xL}\sigma_{x+1,L}\right)^{v_x}, \end{aligned} \quad \text{(A4)}$$

where $H = \sum_y h_y$ and $V = \sum_x v_x$; $h_y = 1$ means the p_{xy} in row y have been flipped. We note that the boundary spins enter only through combinations such as

$\sigma_{1y}\sigma_{1,y+1}\sigma_{Ly}\sigma_{L,y+1}$, which gives the parity of the number of defects in the yth row of the dual lattice. Further, the terms in the sum depend on only four numbers: H; V; the number of rows for which $h_y = 1$ and $\sigma_{1y}\sigma_{1,y+1}\sigma_{Ly}\sigma_{L,y+1} = -1$; and the number of columns for which $v_x = 1$ and $\sigma_{x1}\sigma_{x+1,1}\sigma_{xL}\sigma_{x+1,L} = -1$. Let r be the number of rows for which $\sigma_{1y}\sigma_{1,y+1}\sigma_{Ly}\sigma_{L,y+1} = -1$ and r' be the equivalent number of columns. Then we can write

$$\begin{aligned} Z_\alpha &= 2^{-2L+2}(1+c)^{(L-1)^2} \\ &\times \sum_{h=0}^{r}\sum_{v=0}^{r'}\sum_{h'=0}^{L-1-r}\sum_{v'=0}^{L-1-r'} M^{(1)}_{h,v,h',v'}, \end{aligned} \tag{A5}$$

with

$$\begin{aligned} M^{(1)}_{h,v,h',v'} &= B_{r,h}B_{r',v}B_{L-1-r,h'}B_{L-1-r',v'} \times \\ &(-1)^{h+v} z^{(H+V)(L-1)-2HV}, \end{aligned} \tag{A6}$$

where now $H = h + h'$ and $V = v + v'$ since h and h' are the number of rows with $h_i = 1$ and odd and even defect parities respectively, and v and v' are similar numbers of columns. We denote the binomial coefficients by $B_{n,r} \equiv n!/r!(n-r)!$

We may now sum over v and v', yielding

$$\begin{aligned} Z_\alpha &= 2^{-2L+2}(1+c)^{(L-1)^2} \\ &\times \sum_{h=0}^{r}\sum_{h'=0}^{L-1-r} B_{r,h}B_{L-1-r,h'}M^{(2)}_{h,v}, \end{aligned} \tag{A7}$$

with

$$\begin{aligned} M^{(2)}_{h,h'} &= (-1)^h (z^H + z^{L-1-H})^{L-r'-1} \\ &\times (z^H - z^{L-1-H})^{r'}. \end{aligned} \tag{A8}$$

A similar procedure leads to the expression for the expectation value of any spin, given a boundary condition. We state only the result which depends on the coordinates of the spin $2 \le xy \le L-1$, as well as the total numbers of rows and columns with odd defect parity : r and r'. It also depends on s, the number of such rows with y co-ordinate less than j and s': the number of such columns with x co-ordinate less than i. (Clearly $s \le r$ and $s' \le r'$).

The result is that

$$\langle \sigma_{xy} \rangle = \sigma_{x1}\sigma_{11}\sigma_{1y} Z_\alpha^{-1} M_\alpha, \tag{A9}$$

where

$$M_\alpha = \sum_{h=0}^{s}\sum_{h'=0}^{y-1-s}\sum_{h''=0}^{r-s}\sum_{h'''=0}^{L-y+s-r} M^{(3)}_{h,h',h'',h'''}, \tag{A10}$$

with

$$\begin{aligned} M^{(3)}_{h,h',h'',h'''} = \\ (-1)^{h+h''}(z^H + z^{L-1-H})^{L-x+s'-r'} \times \\ (z^H - z^{L-1-H})^{r'-s'} \times \\ (z^{H-2(h+h')} + z^{L-1-H+2(h+h')})^{x-1-s'} \times \\ (z^{H-2(h+h')} - z^{L-1-H+2(h+h')})^{s'} \times \\ B_{s',h}B_{y-1-s',h'}B_{r'-s',h''}B_{L-y+s'-r',h'''} \end{aligned} \tag{A11}$$

These results are still a little cumbersome, but they are exact, and are can be evaluated computationally. The number of terms in the sum may be as large as $\mathcal{O}(L^4)$, but this is polynomial rather than exponential in the system size.

APPENDIX B: TPM SYMMETRIES AND CONSTRAINTS

Here we make some comments about the thermodynamics of finite $(L \times L)$ droplets in the triangular plaquette model. We first identify the 2^{2L-1} transformations that leave the droplet energy unchanged. Recall that

$$\sigma_{x+1,y} = q_{xy}\sigma_{xy}\sigma_{x,y+1}. \tag{B1}$$

It follows that if we specify the boundary spins σ_{1y} and σ_{xL} (where $x, y = 1 \ldots L$) then the rest of the spins are determined by the set $\{q_{xy}\}$ (with $x, y = 1 \ldots L-1$). Thus, the required degenerate states for a given choice of the $\{q_{xy}\}$ can be generated by cycling through the possible states of these two boundaries.

To identify the constraints on the plaquette variables arising from the boundary conditions, observe that for a ground state ($q_{xy} = 1 \,\forall\, xy$) with specified spins along two boundaries ($\{\sigma_{1y}, \sigma_{xL}\}$) then the state of the remaining boundary spins are

$$\sigma^0_{x1} = \prod_{y=1}^{x} (\sigma_{1y})^{B_{x-1,y-1}}, \tag{B2}$$

$$\sigma^0_{Ly} = \prod_{y'=y}^{L-1} (\sigma_{1y'})^{B_{L-1,y'}} \prod_{x=1}^{y} (\sigma_{xL})^{B_{L-1-x,L-1-y}}, \tag{B3}$$

where $\sigma^{B_{nr}}$ is equal to unity unless $\sigma = -1$ and $B_{n,r}$ is odd, in which case it takes the value -1.

For a general configuration of the q's and the boundary spins σ_{1y}, σ_{xL}, we have

$$\sigma_{x1} = \sigma^0_{x1} \prod_{y=1}^{x-1}\prod_{x'=1}^{x-y} (q_{x'y})^{B_{x-x'-1,y-1}}, \tag{B4}$$

$$\sigma_{Ly} = \sigma^0_{Ly} \prod_{y'=0}^{L-y-1}\prod_{x=1}^{L-y'-1} (q_{y,y+y'})^{B_{L-x-1,y'}}. \tag{B5}$$

Multiplying both sides of each constraint by the appropriate σ^0 leaves an equality between a product of boundary spins and a product of plaquette variable. These are

the $2L-3$ constraints that determine which configurations of the excited plaquettes are present in the partition sum.

While these expressions appear complicated, for a given droplet boundary condition they are simply constraints of the form

$$q_{x_1,y_1}q_{x_2,y_2}\cdots q_{x_n,y_n} = \pm 1, \tag{B6}$$

where the constrained plaquettes form parts of Sierpinski triangles. For example, for $L=4$, the constraint coming from the boundary spin σ_{42} is

$$q_{12}q_{22}q_{32}q_{23} = \sigma_{12}\sigma_{13}\sigma_{24}\sigma_{42}. \tag{B7}$$

In the SPM the constraints were of the form

$$\prod_{y=1}^{L-1} p_{xy} = \pm 1. \tag{B8}$$

The simplicity of (B8) in the SPM, as compared to (B5), is the reason for the relative intractability of the partition function of the TPM.

[1] For reviews on the glass transition see: M.D. Ediger, C.A. Angell and S.R. Nagel, J. Phys. Chem. **100**, 13200 (1996); C.A. Angell, Science **267**, 1924 (1995); P.G. Debenedetti and F.H. Stillinger, Nature **410**, 259 (2001).

[2] T.R. Kirkpatrick and D. Thirumalai, Phys. Rev. Lett. **58**, 2091 (1987); T.R. Kirkpatrick and P. Wolynes, Phys. Rev. B **36**, 8552 (1987); T.R. Kirkpatrick, D. Thirumalai and P. Wolynes, Phys. Rev. A **40**, 1045 (1987)

[3] X. Xia and P.G. Wolynes, Proc. Natl. Acad. Sci. USA **97**, 2990 (2000).

[4] W. Kauzmann, Chem. Rev. **43**, 219 (1948).

[5] M. Mézard and G. Parisi, Phys. Rev. Lett. **82**, 747 (1999); S. Franz and G. Parisi, J. Phys. C **12**, 6335 (2000).

[6] G.H. Fredrickson and H.C. Andersen, Phys. Rev. Lett. **53**, 1244 (1984).

[7] R.G. Palmer, D.L. Stein, E. Abrahams and P.W. Anderson, Phys. Rev. Lett. **53**, 958 (1984).

[8] For reviews on dynamic heterogeneity see: H. Sillescu, J. Non-Cryst. Solids **243**, 81 (1999); M.D. Ediger, Annu. Rev. Phys. Chem. **51**, 99 (2000); S.C. Glotzer, J. Non-Cryst. Solids, **274**, 342 (2000); R. Richert, J. Phys. Condens. Matter **14**, R703 (2002).

[9] For other theories of the glass transition see for example: W. Götze and L. Sjögren, Rep. Prog. Phys. **55**, 55 (1992); D. Kivelson, S.A. Kivelson, X.L. Zhao, Z. Nussinov and G. Tarjus, Physica A **219**, 27 (1995); K. S. Schweizer and E. J. Saltzman, J. Chem. Phys. **119**, 1181, (2003).

[10] J.P. Garrahan and D. Chandler, Phys. Rev. Lett. **89**, 035704 (2002); Proc. Natl. Acad. Sci. USA **100**, 9710 (2003).

[11] S. Whitelam, L. Berthier and J.P. Garrahan, Phys. Rev. Lett. **92**, 185705 (2004).

[12] J. Jäckle and S. Eisinger, Z. Phys. B **84**, 115 (1991).

[13] For a review on kinetically constrained models see F. Ritort and P. Sollich, Adv. Phys. **52**, 219 (2003).

[14] A. Lipowski, J. Phys. A **30**, 7365 (1997)

[15] J.P. Garrahan, J. Phys. Condens. Matter **14**, 1571 (2002).

[16] M.E.J. Newman and C. Moore, Phys. Rev. E **60**, 5068 (1999).

[17] J.P. Garrahan and M.E.J. Newman, Phys. Rev. E **62**, 7670 (2000).

[18] J.P. Bouchaud and G. Biroli, J. Chem. Phys. **121**, 7347 (2004).

[19] P. Scheidler, W. Kob, K. Binder, Euro. Phys. J. E **12**, 5 (2003).

[20] L. Berthier, Phys. Rev. Lett. **91**, 055701 (2003).

[21] We will limit our discussions to typical droplets. One can also study variability in ξ, which is argued could give information about dynamic heterogeneity in the system [18].

[22] D. Espriu and A. Prats, Phys. Rev. E **70**, 46117 (2004).

[23] R. L. Jack, L. Berthier and J.P. Garrahan, Phys. Rev. E **72**, 016103 (2005).

[24] C. Toninelli, M. Wyart, L. Berthier, G. Biroli, J.P. Bouchaud, Phys. Rev. E **71**, 041505 (2005).

[25] T. Castellani and A. Cavagna, J. Stat. Mech. P05012 (2005).